Physical objects approaching the Cauchy horizon of a rapidly rotating Kerr black hole

Caroline Mallary,[1] Gaurav Khanna,[1] and Lior M. Burko[2]

[1]*Department of Physics, University of Massachusetts, Dartmouth, Massachusetts 02747, USA*
[2]*School of Science and Technology, Georgia Gwinnett College, Lawrenceville, Georgia 30043, USA*

(Received 17 July 2018; published 16 November 2018)

We solve the $2+1$-dimensional Teukolsky equation numerically for the Weyl scalars ψ_0 and ψ_4 along a time-like geodesic approaching the Cauchy horizon of a rapidly rotating perturbed Kerr black hole. We find that both the amplitude and frequency of the Weyl scalars agree with the results of linear perturbation analysis. We then model a physical object by a simple damped harmonic oscillator, which is driven by an external force that mimics the tidal force experienced by the infalling object. We use this model to find the total deformation of the object at the Cauchy horizon, and the resonant effect when the driving force's frequency matches the internal frequency of the oscillator that models the object.

DOI: 10.1103/PhysRevD.98.104024

I. INTRODUCTION

The strong cosmic censorship conjecture (SCC) states that given generic compact or asymptotically flat Cauchy data it is impossible to extend the maximal Cauchy development with a Lorentzian manifold equipped with locally square-integrable connections [1]. This formulation of the SCC implies that generic spacetimes will always be globally hyperbolic, and that general relativity retains its deterministic predictability. This definition of the SCC is particularly useful when one seeks to find (possibly weak) solutions of the classical Einstein equations. Indeed, it is hard to see how one would make sense of the Einstein equations if this condition is not satisfied.

However, the Einstein equations break down at singularities, when quantum gravity is expected to take over. That is, one should not be surprised that the classical Einstein equations no longer make sense when curvature becomes super-Planckian, even when the metric is C^0 extendible, as is the case with the mass-inflation singularity [2,3]. From the point of view of an infalling observer, it therefore makes sense to ask whether an observer made of reasonable matter will detect the approach to a spacetime singularity, i.e., whether she will necessarily be destroyed upon approach to the Cauchy horizon (CH). A necessary condition for safe passage across the CH is that the answer to the latter question is in the negative. A definitive answer, however, must await the development of a quantum theory of gravity. In this paper we are interested in investigating this necessary condition for reasonable matter approaching the CH of perturbed isolated Kerr black holes. The rationale of this approach is that if extended physical objects cease to exist, it would be (classically) because of very strong tidal deformations, and while the understanding of how many derivatives of the metric are continuous is extremely important for the mathematical investigation of black hole singularities, it is eventually the physical interactions that determine the infalling objects' fate.[1]

The singularity inside black holes had long been thought to be space-like (like the singularity inside an unperturbed Schwarzschild black hole), and possibly of the Belinskii-Khalatnikov-Lifshitz (BKL) type [4]. Poisson and Israel found that for an isolated spherical charged black hole that is perturbed by its own evolutionary collapse (i.e., by Price tails [5]), a null singularity evolves at the Cauchy horizon [6]. The interaction of an infalling observer with the fields in the interior of a perturbed, isolated, spinning black hole was first considered by Ori [2], who argued, based on the metric and fields being C^0 at the CH, that extended objects might not be destroyed, in the context of a spherical charged toy model perturbed by Price tail radiation. Burko and Ori [7] considered the same model in greater detail, and modeled an infalling object as a (classical or quantum mechanical) undamped oscillator, and then solved for the deviation of the oscillator from its equilibrium length upon arrival at the CH (see also Ref. [8]). In Ref. [7]

[1]One often considers unbounded tidal deformations as the criterion for ultimate destruction. Notice, however, that any physical material is effectively destroyed when experiencing tidal deformations that exceed a certain upper bound that it can tolerate. When tidal deformations are unbounded, any physical object is ultimately destroyed. But if tidal deformations are bounded—even if very large—it becomes a practical engineering problem for materials scientists whether a material that can survive such deformations can be created, not a problem of principle. In other words, we are interested in the question of what the laws of physics forbid, not in what current engineering technology allows.

it was found that such deviations are not just bounded, but even can be as small as one would like if the oscillator is thrown into the black hole sufficiently late. The quantum electrodynamical interaction of blue-shifted cosmic background radiation photons with infalling observers in the same model was addressed in Ref. [9] with similar conclusions. A different approach for finding the interaction of an infalling object with the CH was undertaken by Herman and Hiscock, who considered the increase in internal energy and entropy [10]. (Herman and Hiscock argued that any physical object would be destroyed by such an unbounded increase. See, however, Ref. [11] for a counter argument.) The C^0 extendibility of the CH was placed on firm mathematical ground for the spherical charged case in Ref. [12] and for the Kerr case in Ref. [13].

In this paper we take a similar approach to that taken in Ref. [7] in the context of an isolated Kerr black hole perturbed (linearly) by gravitational waves that result from the Price tails that follow the collapse. We model the (test) infalling object by a damped or undamped oscillator, whose extension $d \ll \mathcal{R}$, where $\mathcal{R}$ is the typical radius of curvature of the background spacetime between the inner and outer horizons. This assumption allows us to ignore the direct effects of curvature inhomogeneities, and instead treat the object as if it were static in a comoving flat laboratory, subjected to gravitational waves that drive the oscillator.

The perturbation source we study here is the same source that was considered in Refs. [2,3,7,8,12–14], specifically the Price tails that continue falling into the black hole a long time after its formation. Astronomical black holes are believed to be perturbed by additional sources, specifically cosmic background radiation photons [9], baryons, and dark matter [15]. Very recently, a perturbation source of collisionless outgoing and ingoing accretion streams was considered in Ref. [16] within a simplifying framework in which spatial gradients are given by a conformally separable solution, possibly beyond the latter's domain of applicability. It was found in Ref. [16] that the singularity evolves into a space-like singularity of possibly the BKL type [4]. We do not consider such perturbation sources here. Obviously, our results and conclusions are valid only for the model under consideration.

The main difference between the force driving the oscillator in the spherical charged and Kerr cases is that in the latter case the driving force is oscillatory, and that the frequency of the oscillations, as measured in the infalling laboratory (the object's proper time τ), grows unboundedly on the approach to the CH, whereas in the former case the driving force is monotonic. As the driving force frequency grows, it matches at one time the oscillator's internal resonance frequency. Here, we consider the resonant effect for the first time.

For specificity, in considering this problem we are loosely motivated by the context of the recent (2014) Hollywood blockbuster movie *Interstellar*, in which the protagonist Cooper, strapped in his spacecraft, freely falls towards the inner horizon of a large, rapidly rotating black hole called Gargantua. In this work, we are motivated by the "tidal" forces experienced by Cooper's spacecraft due to the CH singularity, and calculate it in detail for the black hole model used here, and ask whether it could actually survive the crossing of the inner horizon[2] by examining the strain on his spacecraft. At a later stage in the movie, Cooper ejects from his spacecraft and is shown transitioning into a deeply quantum regime just as he hits Gargantua's inner horizon [17]. We will not consider any quantum effects in this work: our treatment is based entirely on classical general relativity.

II. A SIMPLE MODEL

In this section, following the method of Ref. [7], we introduce the simple physical model that will allow us to compute some of the details of the strain on Cooper's spacecraft through its fall approaching the CH of a rapidly rotating Kerr black hole.

We break this section into two distinct parts. First, we briefly recall the known behavior of physical fields, specifically the gravitational field as one approaches the inner horizon of an isolated, rotating black hole. This first part is largely a review of earlier work [18,19]; therefore, we only emphasize the key differences between previous efforts and this current work. Second, we describe the physical model we use to understand the effect of these fields on a freely falling, (extended) physical object. Henceforth, M refers to the mass of the Kerr black hole and a to its spin parameter. We use standard Boyer-Lindquist coordinates (t, r, θ, φ) and also the usual null coordinates $v = r^* + t$ and $u = r^* - t$ ("advanced and retarded times," respectively) throughout the paper. Our equations are in geometrized units of the black hole, where distance is measured in units of GM/c^2, and time in units of GM/c^3, where G is Newton's constant and c is the speed of light in vacuum.

Ori investigated the behavior of physical fields near the CH using a perturbation analysis approach [3,18,20], and found the asymptotic behavior of the curvature perturbations in terms of the Weyl scalars ψ_4 and ψ_0 at the early portion of the CH to be

[2]It should be noted that in *Interstellar*, Cooper actually approaches the outgoing (or "outflying") sector of the inner horizon that exhibits a shock-wave like singular structure [14]. However, Kip Throne (the science advisor for the movie) did not consider that very natural, given the expected physical parameters of the orbit that Cooper's spacecraft is on [17]. In this work, we will study the more physically natural scenario, i.e., Cooper's spacecraft approaching the CH (or "infalling") sector of the inner horizon. This means that in this paper, the inner horizon's singular structure develops due to gravitational perturbations that *follow* Cooper's spacecraft rather than precede it.

$$\psi_4 \cong u^{-8}(r_- - ia\cos\theta)^{-4} \sum_{m=-2}^{2} A_{m-2} Y_2^m(\theta,\phi) e^{-im\Omega_- u}, \quad (2.1)$$

and

$$\psi_0 \cong (r - r_-)^{-2} v^{-7} \sum_{m=-2}^{2} B_{m2} Y_2^m(\theta,\phi) e^{im\Omega_- v}. \quad (2.2)$$

Here $r_- \equiv M - \sqrt{M^2 - a^2}$, $\Omega_- \equiv a/(2Mr_-)$, $\phi \equiv \varphi - \Omega_- t$ is a regular azimuthal coordinate and ${}_sY_l^m$ are the spin-weighted spherical harmonics. A_m and B_m are coefficients that depend on the initial amplitudes of ψ_4 and ψ_0, respectively. In Ref. [19] some of us verified these results using a direct, numerical approach, i.e., curvature perturbations outside the black hole were directly evolved using linearized equations in the background Kerr spacetime of a rotating black hole. Care was taken to use a coordinate system that allowed the fields to smoothly evolve right through the event horizon and approach the CH along the null direction $u = \text{const}$, $v \to \infty$. In that work, Ori's results were verified numerically to a high degree of accuracy, and new results for the behavior of $\psi_4(u = \text{const}, v)$ were found.

In this current work, we use the same computational setup with one key difference. Instead of approaching the CH along a null geodesic, we approach it along a time-like one. This allows us to directly study the effect of physical fields on a freely falling object as it approaches the CH of a rotating black hole.

In the context of a rotating black hole, it was shown in Ref. [18] that the most divergent components of the Riemann curvature tensor are proportional to ψ_0, as given in Eq. (2.2). Ori predicted that the "tidal" forces on an infalling object would behave as the real part of

$$\tau^{-2}[\ln(-\tau/M)]^{-7} \sum_{m=1,2} C_{m2} Y_2^m(\theta_0,\phi_0) e^{-imp\ln(-\tau/M)} \quad (2.3)$$

where τ is the proper time associated to the falling object chosen such that $\tau = 0$ is when the object hits the CH, and θ_0, ϕ_0 are the angular positions at which the object hits the CH. Here, $p \equiv a(M^2 - a^2)^{-1/2}$. This expression for the tidal forces is valid when the object is close to the inner horizon, i.e., when τ has a sufficiently small negative value.

Ori argued that the tidal deformations described by Eq. (2.3) would stay finite [3], thus making the CH singularity a weak one in Tipler's classification [21]. (See also Ref. [22].) It was also noted in Ref. [3] that the object would experience infinitely many oscillations, with ever increasing frequency. We verify below all of these expectations by performing direct numerical computations.

To study the effect of the tidal forces on an infalling extended object, we consider a basic oscillator as a physical toy model for an extended object. The oscillator is parametrized by mass μ, spring constant k, and damping coefficient b. Our mathematical model for the infalling object will be given by

$$\mu\ddot{x} + b\dot{x} + kx = F(\tau), \quad (2.4)$$

where $x(\tau)$ is proportional to the strain experienced by the object (at equilibrium length $x = 0$). The driving force $F(\tau)$ is chosen proportional to the expression (2.3). In the next section we show that our numerical results for ψ_0 corroborate this expression for $F(\tau)$, and find $x(\tau)$ throughout the fall. We align the model object so that it responds to the driving force in full magnitude, i.e., the infalling spacecraft uses its engines to align itself so that it does not rotate.

III. COMPUTATIONAL RESULTS

We begin this section with a brief description of our numerical setup. As pointed out in the previous section, we take an approach similar to the one described in detail in Ref. [19]. In particular, we numerically solve the Teukolsky equation for ψ_0 and ψ_4 in specifically designed compactified, ingoing-Kerr coordinates that allow us to "penetrate" the horizons and also provide us with great computational efficiency. The initial field configuration is a Gaussian profile located outside the horizon, centered at $r = 8M$ and of width $M/10$. The angular distribution of the initial field corresponds to $\ell = m = 2$. Other numerical parameters and details of the numerical scheme utilized may be found in Ref. [19]. As the computation evolves the fields are sampled along a time-like geodesic. For the results depicted below, equatorial geodesics with $E/\mu = 1$, $L/\mu = 2M$ were used; however, the main features of our results appear to be applicable to other time-like geodesics. In Fig. 1 we show a plot for the late portion of the time-like geodesics we used for two Kerr black holes with spin parameters $a/M = 0.8$ and 0.9165.[3]

A. Oscillatory singularity

In Figs. 2 and 3 we show the results of our numerical simulations, alongside the results of perturbation analysis [18] for the time-like geodesics shown in Fig. 1. There is clear agreement between the two results, especially at late times; note that the overall amplitude and phase were adjusted to obtain this match, and that the agreement is maintained over more than 50 orders of magnitude. At early times, we do not expect to see a close match between the two results because in Ref. [18] multiple near-horizon approximations were used in the analysis, whereas our results also capture subdominant modes.

[3]In *Interstellar*, Gargantua's mass is $M_{\rm Gar} \sim 1$–$2 \times 10^8\, M_\odot$ and its spin parameter is $(a/M)_{\rm Gar} \sim 1 - \varepsilon$, where $\varepsilon \sim 1.3 \times 10^{-14}$ [17]. Such closeness to extremality is difficult to simulate numerically, and so in practice we simulate lower values for a, although we still solve for a fast-spinning Kerr black hole.

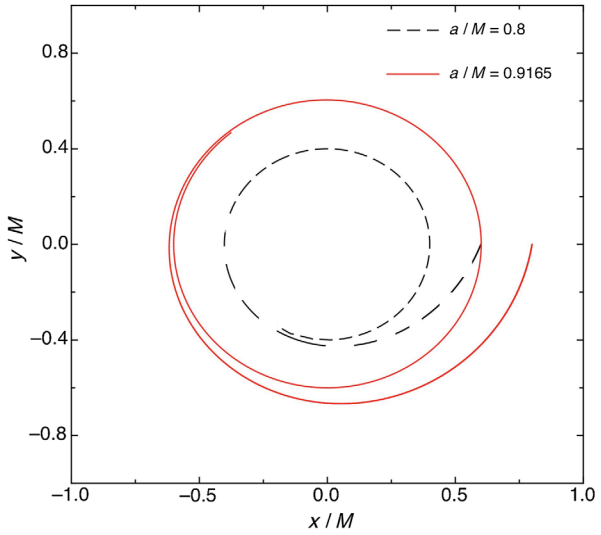

FIG. 1. The $E/\mu = 1$, $L/\mu = 2M$, equatorial, time-like geodesics for two black holes with spin rates $a/M = 0.8$ or 0.9165. The inner horizons are, correspondingly, at $r_- = 0.4M$ or $0.6M$. We depict the late-stage portion of these geodesics.

It is clear that at late times, i.e., in close proximity to the CH, curvature grows with an inverse-square power of τ. (Recall that $\tau < 0$ and approaches zero). This unbounded growth of curvature is the physical manifestation of the failure of the manifold to have square-integrable connections in any neighborhood of the CH. Naively, one may interpret that growth rate as a divergence that would destroy any object that is unfortunate enough to approach it. We address this issue in Sec. III B. In addition, notably the frequency of oscillation monotonically increases with proper time τ upon approach to the CH. In fact, the instantaneous frequency can easily be computed to be

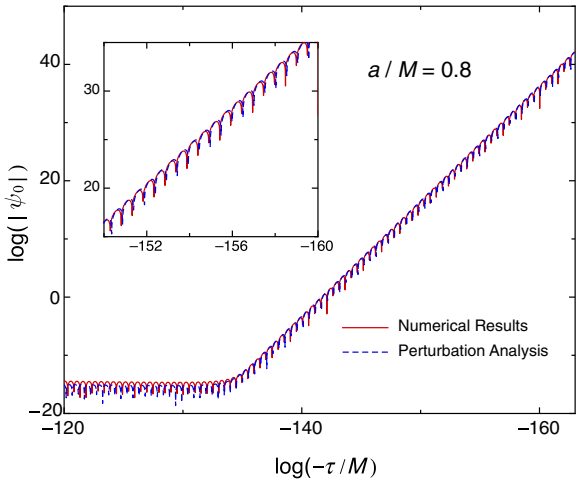

FIG. 2. The curvature scalar ψ_0 as a function of the proper time of a time-like observer falling into a Kerr black hole with $a/M = 0.8$. The logarithms are base 10. Our numerical results are depicted by a solid curve, and the perturbation analysis prediction of Ref. [18] is shown with a dashed curve.

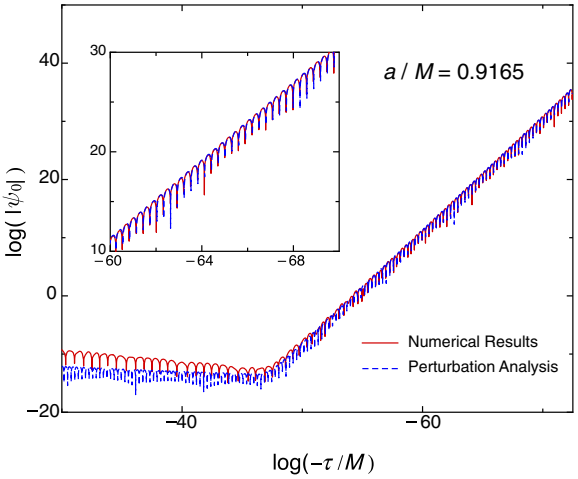

FIG. 3. Same as Fig. 3 for $a/M = 0.9165$.

$\omega(\tau) = 2p/(-\tau)$. Thus, the infalling object experiences ever stronger tidal forces and with faster oscillatory cycles as it approaches the CH.

B. Extended physical object

We use the simple oscillator model (2.4) to understand the effects of the tidal forces (2.3) on a material object.

First, consider the form of the forcing function $F(\tau)$ in Eq. (2.4). This expression should be proportional to the tidal force given in the formula (2.3). For simplicity, we focus on the $\ell = 2$, $m = 2$ harmonic, which is the dominant harmonic near the black hole's equator. We are concerned with the real part of the expression (2.4), so the $e^{-\mathrm{imp}\log(-\tau/M)}$ factor can be simplified to $\cos[mp\ln(-\tau/M)]$. The $\ell = 2$, $m = 2$ harmonic Y_2^2 is proportional to a constant, so we are left with the driving force

$$F(\tau) = F_0\tau^{-2}[\ln(-\tau/M)]^{-7}\cos[2p\ln(-\tau/M)] \qquad (3.1)$$

where F_0 is some constant that depends on the details of the actual physical origin of the black hole perturbation and the time that has elapsed since it formed or since its mass has increased until the object crosses its event horizon. The calculation of F_0 is outside the scope of this work, so we will treat it as an overall scaling constant for the strain. In practice, our results for the strain are the strain per F_0.

In geometrized units the parameters of the oscillator (2.4), μ, b, and k, turn out to be many orders of magnitude apart, for any realistic oscillating matter falling into a supermassive black hole like Gargantua. Recall that the parameters μ, b, and k have fixed values associated to the properties of the infalling object. Furthermore, $F(\tau)$ oscillates rapidly as $\tau \to 0^-$. The equation is stiff and difficult to simulate.

We can facilitate the simulation by replacing τ with a new time variable s, where $s \equiv -M\ln(-\tau/M)$ ("logarithmic time"), for which the object hits the CH as $s \to \infty$. The

use of s as the time variable requires some alteration to the form of Eq. (2.4), since the strain x will now be expressed as a function of s rather than τ. We can rewrite Eq. (2.4) as

$$\mu x'' + \left(\frac{\mu}{M} + be^{-s/M}\right)x' + e^{-2s/M}kx = -\frac{F_0 M^5 \cos\frac{2ps}{M}}{s^7} \tag{3.2}$$

where x'' and x' refer to the derivatives of x with respect to logarithmic time s.

1. Analytical approximation

In addition to being easier to simulate, this form of the oscillator (3.2) makes it easier to set some qualitative expectations of what may happen as the falling object approaches the CH. The forcing function on the right-hand side maintains a constant frequency of $2p/M$ when s is the time coordinate. However, the forcing function decreases in magnitude rapidly. At large values of s the oscillator (3.2) can be reduced to the trivial form $x''(s) + x'(s) \cong 0$. This implies that the "strain" $x(s)$ has an exponentially decaying solution (to a constant asymptotic value) as $s \to \infty$.

However, this exponentially decaying strain does not rule out the possibility of an interesting phenomenon at a somewhat earlier time; specifically, note that while the forcing frequency is a constant $\omega(s) = 2p/M$, the effective natural frequency of the object is not constant. Recall that the x term of a standard driven oscillator equation (2.4) is proportional to the natural frequency squared ($k = \mu\omega_0^2$). In our altered oscillator equation (3.2), the $x(s)$ term is instead proportional to $e^{-2s/M}k$. That is, $\mu\tilde{\omega}_0^2 \equiv e^{-2s/M}k$, where $\tilde{\omega}_0$ is the effective natural frequency, and

$$\tilde{\omega}_0 = e^{-s/M}\sqrt{k/\mu}. \tag{3.3}$$

This result suggests that the natural frequency effectively decreases with logarithmic time s. At some point during the object's fall, its effective natural frequency $\tilde{\omega}_0$ may be equal to the forcing frequency $\omega(s)$. This occurs at logarithmic time

$$\tilde{s} = -M \ln\left[\frac{2p}{M}\sqrt{\frac{\mu}{k}}\right]. \tag{3.4}$$

We expect that as $s \simeq \tilde{s}$, a resonance-like effect may occur. Such an effect may result in a momentary increase in the strain on the falling observer. We direct our attention to these expectations in our numerical results that appear below.

2. Numerical results

Our numerical simulations consist of solving Eq. (3.2) for different input parameters. We primarily used MATLAB R2017A's built-in stiff ordinary differential equation (ODE) solvers. Care must be taken when solving ODEs like Eq. (3.2): simulations which are set up incorrectly can yield very different results when different methods are used, or when simulating forward or backward in time. To ensure accuracy, we present results which were nearly identical for all ODE solvers tested. As a check, we simulated both forward and backward in time, to ensure convergence in the region of interest. Finally, we checked our results against results from the `ParametricNDSolve` function in MATHEMATICA 11.

The four MATLAB ODE solvers tested were `ode15s`, `ode23s`, `ode23t`, and `ode23tb`.[4] These solvers do not have a fixed step size. Instead, they use numerical derivatives to estimate an appropriate step size adaptively. When MATLAB was allowed to choose the step size, the different solvers did not give converging results. However, if the solvers' `MaxStep` option is set to a sufficiently low value, results either converge, or the solvers fail entirely and do not run. We found that `ode23s` and `ode23tb` converged at MaxStep $= 10^{-3}M$ or lower, and `ode15s` and `ode23t` failed entirely (see Fig. 5).

We also checked whether `ode23s` gave the same result when evolved forward in time (in the $+s$ direction) and backward in time (the $-s$ direction). The $-s$ evolution tends to diverge from the $+s$ evolution at low s, but is well behaved for lower values s when `MaxStep` is further reduced.

For specificity, we choose a fast-spinning Kerr black hole, with $a/M = 0.995$ ($p = 10$), and choose the timelike geodesic to have $E/\mu = 1$ and $L/\mu = 4M$. The shape of this geodesic is shown in the Penrose diagram in Fig. 4. Our choice of the input material parameters (μ, b, k) is much more open. The vibration of the infalling object sweeps across an infinite range of frequencies of the incoming gravitational waves: it is easy to design inputs that meet the resonance condition at some point during the infall. However, not all such input parameters are physically reasonable, and it can be difficult to intuit what physically reasonable parameters look like when working in the natural units of a black hole. We would like to demonstrate that the resonance conditions can be met by realistic objects, and are not just a mathematical curiosity that may only be relevant to unrealistic matter. To that end, we present results where μ, b, k are set to values corresponding to actual materials.

First, we choose the parameters to roughly correspond to a 1 m^3 steel block, whose vibrations are damped at 1/4 of critical damping ($\zeta = \frac{1}{4}$). Here, the damping ratio $\zeta := b/(2\sqrt{\mu k})$. These parameters are listed in Table I.

[4] `ode15s` is a variable-step, variable-order solver based on the numerical differentiation formulas of orders 1 to 5. `ode23t` is an implementation of the trapezoidal rule using a free interpolant. `ode23s` is based on a single-step modified Rosenbrock formula of order 2. `ode23tb` is an implicit Runge-Kutta formula with a trapezoidal rule step as its first stage and a backward differentiation formula of order 2 as its second stage. See Ref. [23].

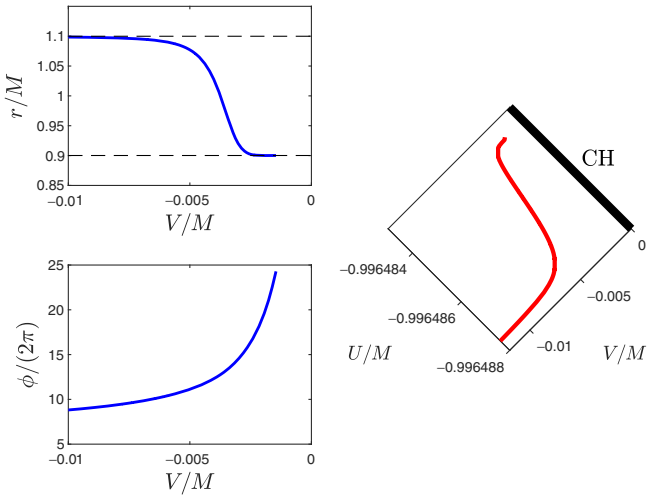

FIG. 4. The path of an object with $E/\mu = 1$ and $L/\mu = 4M$ falling toward the CH of a Kerr black hole with $M = 10^6\ M_\odot$ and $a/M = 0.995$ ($p = 10$) on the equatorial plane. The CH is at Kruskalized advanced time $V = 0$. Top left panel: r as a function of V. The event and inner horizons are shown as dashed lines. Bottom left panel: ϕ as a function of V. Right panel: The Penrose diagram. It is as yet unknown whether there is a continuation of the spacetime manifold beyond the CH (thick line). Notice, that the Kruskalized retarded time U has been stretched in the Penrose diagram to show the curvature in the world line. Because of the scale of the diagram the event horizon (at $U/M = -1$) or future null infinity $\mathcal{I}^+$ are not shown on the Penrose diagram.

The middle column of Table I shows the parameters in MKS units, while its last column shows the same values, as converted into the geometrized units of a black hole with $M = 10^6\ M_\odot = 2 \times 10^{36}$ kg.

Notice that in geometrized units of a supermassive black hole, the parameters of an ordinary object may be quite small, as is the case for the steel cube. We estimate that in order to see resonance, we need the expected resonance logarithmic time $\tilde{s}$ to attain a positive value [see Eq. (3.4)]. Therefore, the size of the parameters is less relevant than the ratio of μ, k, and p. For a high-spin black hole (e.g., $p = 10$ or $a/M = 0.995$), k must be several orders of magnitude higher than μ in order for $\tilde{s}$ to be positive. This is the case for the steel cube parameters, for which $\tilde{s} = 7.06M$. Although we could choose μ and k to be larger numbers, there is little to be gained in terms of either mathematical elegance or realism. Note, however, that to make a precise prediction we would be required to have at least an order-of-magnitude estimate for F_0 in Eq. (3.2).

TABLE I. Parameters for a 1 m^3 of damped 1020 steel, for $10^6\ M_\odot$ black hole.

Parameter	MKS values	Geometrized values
μ	7870 kg	3.935×10^{-33}
$b(\zeta = \frac{1}{4})$	1.913×10^7 N/(m/s)	4.738×10^{-29}
k	186 GPa · m [a]	2.282×10^{-24}

[a]Calculated using $k = YA/L$, where Y is Young's modulus and A and L are the area and length of the cube, respectively. Data are from Ref. [24].

The object's oscillation is directly proportional to F_0, but we are agnostic here as to the magnitude of F_0, because there are many possible sources for the perturbations of the black hole, e.g., the remnant of fields associated with the collapse process, accreted matter from a surrounding disk, perturbations from an orbiting spacecraft, photons coming from the cosmic background radiation, etc. Therefore, the results of our simulation of Eq. (3.2) are normalized so that the peak oscillation amplitude is unity. The normalization factor is 7.4166×10^{-25}. The smallness of the normalization factor will become pivotal for our conclusions below. These results are shown in Fig. 5. Note, however, that for an object that falls into the black hole a long time after the latter has formed (from a collapse process or a long time after its mass has increased otherwise) and has been unperturbed otherwise, the effective magnitude of F_0 is very small due to the exponential decay of quasinormal modes followed by a Price power-law tail. We have not factored out such a decrease in the magnitude of F_0 here. For an old black hole (i.e., a black hole which is unperturbed since formation), such as Gargantua, the normalization factor will therefore be much smaller than the one we are using here. The magnitude of our normalization factor is perhaps more relevant for a young black hole, i.e., for an object that falls into the black hole only a short time after the latter has formed. In this sense our results are upper bounds on the response of the infalling object.

Second, for comparison we change the parameters for an object made of a different material and having a different

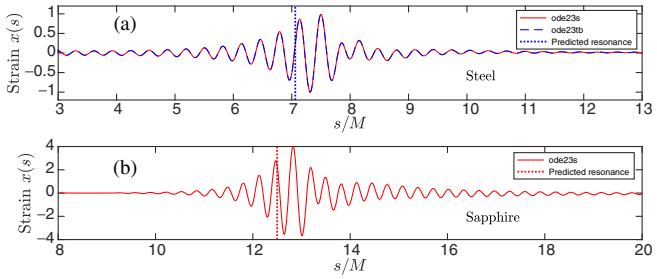

FIG. 5. The normalized strain of a 1 m^3 cube of 1020 steel [top panel, (a)] and on a 1 m^2 × 0.01 m thick plate of single-crystal sapphire [bottom panel, (b)], as they approach the CH of a Kerr black hole as functions of logarithmic time s. In the top panel (a) the simulation is done using both MATLAB's `ode23s` and `ode23tb` methods with `MaxStep` set to $10^{-3}M$. In the bottom panel (b) the simulation is done using MATLAB's `ode23s` method with `MaxStep` set to $10^{-3}M$. In both panels the expected time of resonance is indicated with dotted lines. The results are normalized so that the peak strain of the steel cube is unity. Note, that the strain x is shown here (and also in Figs. 6 and 7) in geometrized units.

TABLE II. The parameters for a 1 m^2 by 0.01 m thick plate of single-crystal sapphire, damped, for a 10^6 $M_\odot$ black hole.

Parameter	MKS values	Geometrized values
μ	39.7 kg	1.985×10^{-35}
$b(\zeta = \frac{1}{4})$	2.160×10^7 N/(m/s)	5.349×10^{-29}
k	470 GPa · m [a]	5.767×10^{-22}

[a]Calculated using $k = YA/L$, where Y is Young's modulus and A and L are the area and thickness of the plate, respectively. Data are from Ref. [25].

shape. In Table II, we consider a 1 $m^2 \times 1$ cm plate of single-crystal sapphire (Al_2O_3), for which the interaction is across the thin side. This material can be used in aerospace viewing windows, so we could imagine this plate as a window in a spacecraft. As with the steel cube, we are able to predict the resonance time of $\tilde{s} = 12.5M$ with reasonable accuracy. The results for the sapphire plate window are also shown in Fig. 5. It is apparent that the steel cube and sapphire plate window behave qualitatively similarly, and that both resonate in predictable but distinct times.

We may also wish to consider the role of damping in this oscillation. Removing the damping from the steel cube (the model considered in Ref. [7]), we observe the expected higher amplitude of oscillation, as shown in Fig. 6. There are also some differences in the frequency composition, which are most obvious at times later than the resonance.

To see the early-time differences between the damped and undamped oscillations, it is best to view the data in proper time τ instead of the logarithmic time coordinate s. Figure 7 is the same as Fig. 6, but shown in τ. Additionally, Fig. 7 contains an inset showing the detail of the damped versus undamped oscillation at low τ. We see that the undamped oscillations include undulations which appear to have a constant period in τ, not s. These oscillations can be measured to have a period of about 2.6×10^{-4} in τ, which

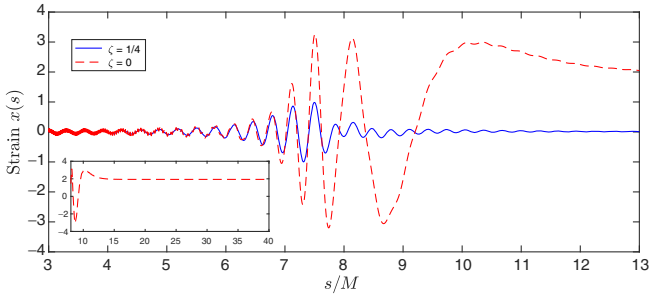

FIG. 6. The damped ($\zeta = 1/4$, solid) and the undamped ($\zeta = 0$, dashed) strains on the steel cube as functions of logarithmic time s. The inset shows the undamped case at later values of s than is shown in the main figure. The scaling is chosen so that the maximum strain of the damped case has unity value. The maximum strain of the undamped case on this scale is 3.2585, and the undamped oscillator settles to a permanent strain of 0.5935 of its maximum strain.

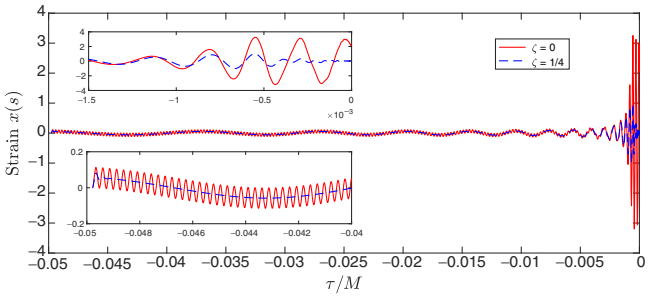

FIG. 7. The damped ($\zeta = 1/4$, dashed) and the undamped ($\zeta = 0$, solid) strains on the steel cube as functions of proper time τ. The insets show zoom-ins for early and late proper times. The scaling is chosen so that the maximum strain of the damped case has unity value.

implies an angular frequency of $\omega(\tau) \approx 2.4 \times 10^4$. We note that in the time domain, our steel cube has an analytic natural frequency of $\omega_0(\tau) = \sqrt{\frac{k}{\mu}} = 2.4082 \times 10^4$, similar to the measured frequency of these undulations. It appears that in the absence of damping, an infalling object may vibrate near its natural frequency even before resonance occurs. The resonance will occur when the frequency of the driving force and this natural frequency approximately coincide.

IV. CONCLUDING REMARKS

We have shown that the total integrated deformation for a simple model of a realistic physical object approaching the CH of an isolated spinning black hole which is perturbed by the Price tails of radiation that follow the collapse process is bounded, and that the maximal deformation may be obtained well before hitting the CH, when the incoming gravitational waves are in resonance with the object's natural frequency. The actual deformation depends on the parameter F_0, which in turn depends on the perturbing field of the black hole and the age of the black hole at the moment the infalling object crosses the event horizon. One should bear in mind that in addition to the deformation itself, any physical object would also undergo successive oscillations, which may undermine its integrity and strength if they are violent enough. In practice, the survivability of the material depends on the interplay of the material's relaxation time with the strain rate and the oscillation frequency. However, we predict that these deformations and oscillations are quite small.

Our interaction model is very simplistic. A realistic object would experience tidal deformations along all three axes, so that the object is successively stretched along one direction and compressed in the other directions. Also, because of the effect of dragging of inertial frames, such an object will generally rotate, so that the direction along which the tidal forces act will change. One approach to address this effect would be to solve for the Jacobi fields

along the object's world line to find the time behavior of the volume element. We do believe, however, that our very simple physical model captures the essential part of the tidal deformation of a realistic object approaching the CH of a black hole within the model used.

This paper does not address the deformation suffered by objects that approach the outgoing leg of the black hole's inner horizon, where one expects to find the Marolf-Ori "outflying" singularity [14]. This paper also does not address other perturbation sources such as baryons and dark matter from accretion processes, and irradiating photons from the cosmic background radiation, specifically those associated with an asymptotically de Sitter universe. Recently there has been renewed interest in the SCC in the context of black holes that are immersed in de Sitter spacetime [26,27]. A detailed interaction model for the Kerr–de Sitter case is awaiting further investigation.

Finally, we have addressed the interactions until the moment that the infalling object hits the CH. It is as yet an open question whether, within the model studied here, there is a classical continuation of the spacetime manifold beyond the CH, perhaps following a short transitional regime where quantum gravity effects are important, and whether physical objects could survive this transition.

ACKNOWLEDGMENTS

We thank Amos Ori for discussions at an early stage of this project, and for valuable comments made on an earlier draft. We thank Kip Thorne, Jay Wang, and Scott Field for discussions. C. M. acknowledges research support from the University of Massachusetts Dartmouth Graduate School. G. K. acknowledges research support from NSF Grant No. PHY–1701284, and from the U.S. Air Force Agreement No. 10–RI–CRADA–09.

[1] D. Christodoulou, *The Formation of Black Holes in General Relativity*, EMS Monographs in Mathematics (European Mathematical Society, Zürich, 2009).
[2] A. Ori, Phys. Rev. Lett. **67**, 789 (1991).
[3] A. Ori, Phys. Rev. Lett. **68**, 2117 (1992).
[4] V. A. Belinskii, I. M. Khalatnikov, and E. M. Lifshitz, Adv. Phys. **19**, 525 (1970).
[5] R. H. Price, Phys. Rev. D **5**, 2419 (1972).
[6] E. Poisson and W. Israel, Phys. Rev. D **41**, 1796 (1990).
[7] L. M. Burko and A. Ori, Phys. Rev. Lett. **74**, 1064 (1995).
[8] L. M. Burko, arXiv:gr-qc/9801018.
[9] L. M. Burko, Phys. Rev. D **55**, 2105 (1997).
[10] R. Herman and W. A. Hiscock, Phys. Rev. D **46**, 1863 (1992).
[11] A. Ori, in *Internal Structure of Black Holes and Spacetime Singularities*, Annals of the Israel Physical Society Vol. 13, edited by L. M. Burko and A. Ori (Institute of Physics, Bristol, 1997), pp. 516–530.
[12] M. Dafermos, Commun. Pure Appl. Math. **58**, 445 (2005).
[13] M. Dafermos and J. Luk, arXiv:1710.01722.
[14] D. Marolf and A. Ori, Phys. Rev. D **86**, 124026 (2012).
[15] A. J. S. Hamilton and P. P. Avelino, Phys. Rep. **495**, 1 (2010).
[16] A. J. S. Hamilton, Phys. Rev. D **96**, 084041 (2017).
[17] K. S. Thorne, *The Science of Interstellar* (W. W. Norton & Company, New York, 2014).
[18] A. Ori, Phys. Rev. Lett. **83**, 5423 (1999).
[19] L. M. Burko, G. Khanna, and A. Zenginoğlu, Phys. Rev. D **93**, 041501(R) (2016); **96**, 129903(E) (2017).
[20] A. Ori, Phys. Rev. D **61**, 024001 (1999).
[21] F. J. Tipler, Phys. Lett. **64A**, 8 (1977).
[22] A. Ori, Phys. Rev. D **61**, 064016 (2000).
[23] MatLab R2018b web documentation, section on stiff-ODEs, https://www.mathworks.com/help/matlab/math/solve-stiff-odes.html.
[24] MatWeb, database of material properties, http://www.matweb.com.
[25] Kyocera sapphire crystal properties, https://global.kyocera.com/prdct/fc/product/pdf/s_c_sapphire.pdf.
[26] V. Cardoso, J. L. Costa, K. Destounis, P. Hintz, and A. Jansen, Phys. Rev. Lett. **120**, 031103 (2018).
[27] O. J. C. Dias, F. C. Eperon, H. S. Reall, and J. E. Santos, Phys. Rev. D **97**, 104060 (2018).